International Journal of Heat and Mass Transfer 52 (2009) 2552–2564

Contents lists available at ScienceDirect

International Journal of Heat and Mass Transfer

journal homepage: www.elsevier.com/locate/ijhmt

Shaker-based heat and mass transfer in liquid metal cooled engine valves

Wolfgang Sander, Bernhard Weigand *

Institut für Thermodynamik der Luft-und Raumfahrt (ITLR), Universität Stuttgart, Pfaffenwaldring 31, 70569 Stuttgart, Germany

ARTICLE INFO

Article history:
Received 10 January 2008
Received in revised form 24 September 2008
Available online 23 February 2009

Keywords:
DNS
VOF
Engine valve
Shaker-effect
Liquid sodium cooling

ABSTRACT

The highly transient process of the working combustion engine generates a "shaker-effect" inside the hollow valve stem where liquid sodium carries the heat from the hot valve head to the valve stem. Here it can pass through the valve guide, based on convective heat transfer and thermal conduction. The efficiency of these transport mechanisms is still not clearly understood, since the design of many liquid cooled valves is mostly based on empirical knowledge and can lead under certain conditions to a breakdown of the system. A simulation of the processes during the movement of the valve including detailed insight into the highly transient and complex two-phase flow phenomena as well as the heat transfer has been realized by means of direct numerical simulation (DNS) based on the volume-of-fluid (VOF) method. The influence of several relevant influencing factors such as the geometry, the acceleration and the liquid fill level were studied. It was found that the fill level is one of the most influencing factors regarding the efficiency of the heat transfer whereas the influence of geometrical dimensions and in particular the aspect ratio of the cavity were almost negligible in our setup. By averaging the fluid flow and the temperature field it has been shown that liquid cooled valves are more efficient compared to a solid valve but clustering of the liquid filling can appear which causes a temporal breakdown of the "shaker-effect". In addition the influence of the spatial resolution is shown and 2D vs. 3D simulation setups are compared. To our knowledge, no similar heat transfer predictions of the presented type are published in the literature.

1. Introduction

The design of combustion engines has always been subject to numerous restrictions and demands which limit the increase of their efficiency and durability. In particular, thermal loads caused by the combustion process and mechanical stresses caused by the valve train were two of the most restricting factors when increasing the power, speed and torque of piston engines during the early 1900s. Newer downsizing concepts where small and lightweight components must be designed can lead to severe thermal conditions which require efficient cooling mechanisms. The improvement of cooling mechanisms and the inherent requirement to increase the durability of combustion engines are therefore two of the most important subjects for new design concepts of modern combustion engines.

During engine operation the exhaust valve opens and heats up since hot exhaust gas flows around the valve head. When closing, the valve contacts the valve seat and heat is transferred out via the valve seat by means of heat conduction. If the heat transfer based on these mechanisms is not balanced, the valve can overheat. For this reason solid steel exhaust valves are a limiting component since the alloys used are not durable under the highest temperatures and accelerations. The breakthrough was the invention of an internally cooled valve by Sam Heron. He introduced a liquid-filled cavity to carry heat from the hot valve head to the cooler stem. First water and then mercury were used as coolants; after difficulties with both these liquids, sodium was found to be an ideal working fluid because of its thermal properties within the operating temperature range.

Valves at the inlet and the outlet of the combustion chamber in modern combustion engines must withstand very high accelerations in the order of several hundred times the earth gravitational constant g, depending on the camshaft profile and the engine revolutions. Valves at the outlet of the combustion chamber must be durable at high temperatures of ≈1000 °C as well. Apart from this, it is also important to reduce the accelerated mass, which affects the wear and the efficiency of the valve train. Thus, industry has developed a new generation of engine valves based on liquid sodium cooling (see Fig. 1). Since sodium inside the hollow valve melts at ≈97 °C during engine operation it can be used as working fluid in order to improve the heat transfer in the valve. This cooling technique is very effective at high temperatures because the heat from the valve head near the combustion chamber is transported into the cold region close to the valve guide and the camshaft. Heat

* Corresponding author. Tel.: +49 711 685 3590; fax: +49 711 685 2317.
E-mail addresses: wolfgang.sander@itlr.uni-stuttgart.de (W. Sander), bw@itlr.uni-stuttgart.de (B. Weigand).

0017-9310/$ - see front matter © 2009 Elsevier Ltd. All rights reserved.
doi:10.1016/j.ijheatmasstransfer.2008.09.045

Nomenclature

a	thermal diffusivity ($m^2\ s^{-1}$)
a_v	valve acceleration ($m\ s^{-2}$)
c_p	specific heat at constant pressure ($J\ kg^{-1}\ K^{-1}$)
D_h	hydraulic diameter (m)
e_{kin}	kinetic energy (J)
f	volume of fluid
g	gravitational acceleration ($m\ s^{-2}$)
H	channel height (m)
i	index in x-direction
j	index in y-direction
k	index in z-direction
k	thermal conduction ($W\ m^{-1}\ K^{-1}$)
$\mathbf{k}$	acceleration vector ($m\ s^{-2}$)
l_v	valve lift (m)
L	channel length (m)
m	mass (kg)
p	pressure (Pa)
$\dot{\mathbf{q}}$	heat flux vector ($W\ m^{-2}$)
t	time (s)
$\boldsymbol{T}$	capillary stress tensor ($N\ m^{-2}$)
T	temperature (K)
T_h	high temperature (K)
T_0	low temperature (K)
$\boldsymbol{u}$	velocity vector ($m\ s^{-1}$)
v_v	valve velocity ($m\ s^{-1}$)
V	volume (m^3)
$\boldsymbol{x}$	Cartesian coordinates (x,y,z)

Greek symbols

μ	dynamic viscosity ($kg\ m^{-1}\ s^{-1}$)
ρ	density ($kg\ m^{-3}$)
σ	surface tension ($N\ m^{-1}$)
Θ	normalized temperature, $\frac{T-T_0}{T_h-T_0}$

Subscripts

g	gaseous phase
l	liquid phase
y	vertical direction

Superscripts

rms	root mean square
c	conduction

transfers out of the liquid sodium through the valve stem (10), the valve guide (4), and finally the engine coolant around the water cooling passage (9) or the lubricating oil.

The periodic nature of the valve movement which maintains this cooling technique can be divided in two periods: (i) the acceleration period during the opening and closure of the valve, which accelerates the liquid depending on the liquid fill level, followed by (ii) the stationary period where the flow is driven by inertial forces. This process, similar to a shaker, drives the transport mechanism inside the hollow valve. Thus, this effect, which leads to a better distribution of the heat in the valve by avoiding extremely hot areas in the valve stem, is often called the "shaker-effect". The highly transient movement of the liquid flow is characterized by strong three-dimensional fragmentations resulting in drastic topological changes of the liquid phase during the acceleration of the valve and merging based on coalescence during the stationary period. Thus, it is very difficult to observe these phenomena experimentally and take heat transfer measurements.

The essential idea of direct numerical simulation (DNS) is to approach the continuum flow with an extremely fine spatial resolution without using any turbulence model. Hence, it is not necessary to know a priori whether the flow is laminar or turbulent

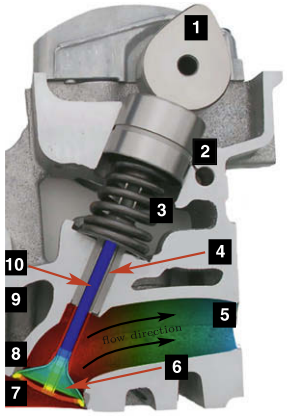

1. camshaft
2. oil lubrication/cooling
3. valve spring
4. valve guide
5. exhaust
6. valve head
7. combustion chamber
8. valve seat
9. water cooling passage
10. hollow valve stem

Fig. 1. Valve train assembly (outlet side) – see Wikipedia [17].

because all length scales of the flow up to the order of the mesh size are captured by the direct simulation. Even very short time scales, depending on the mesh size with respect to the Courant–Friedrichs–Levy (CFL) condition, are captured by DNS. Therefore it is reasonable to simulate the flow and heat transfer based on DNS. Although these mechanisms are very important for the design of internally cooled exhaust valves, no other results regarding the flow field and heat transfer predictions are presently given in the literature.

Preliminary results obtained from simplified 2D-simulations which were published in Sander et al. [15] have shown that the mixing mechanism of the two-phase flow and the dynamically changing liquid distribution inside the valve are characteristic of shaker-based heat transfer. In particular the kinetic energy of the liquid phase and the heat flux in axial direction, which indicate the efficiency of the shaker-based heat transfer, were studied at different liquid fill levels. The new 3D-simulation results obtained allow observing small details inside the flow, where experimental setups often fail because of a lower spatial and temporal resolution capability.

Due to an improved performance of the program and increased computational resources the focus of the present study was directed to identify 3D-effects appearing in the flow for longer run-times up to 400 revolutions. Different configurations were considered in order to identify the influence on the heat transfer efficiency caused by several factors such as the liquid fill level, the geometry of the hollow valve stem and the nature of the valve acceleration.

2. Numerical method

The flow is governed by the Navier–Stokes equations for incompressible flows and the energy equation (Eqs. (1)–(3)).

$$\frac{\partial \rho}{\partial t} + \nabla \cdot (\rho \mathbf{u}) = 0, \tag{1}$$

$$\frac{\partial (\rho \mathbf{u})}{\partial t} + \nabla \cdot (\rho \mathbf{u}) \otimes \mathbf{u} = -\nabla p + \nabla \cdot \mu \left[(\nabla \mathbf{u} + (\nabla \mathbf{u})^T) \right] + \rho \mathbf{k} + \nabla \cdot \mathbf{T}, \tag{2}$$

$$\frac{\partial(\rho c_p T)}{\partial t} + \nabla \cdot (\rho c_p \mathbf{u} T) = \nabla \cdot (k \nabla T) \tag{3}$$

where $\mathbf{u}$ denotes the velocity vector, t, the time, ρ, the density, μ, the dynamic viscosity, p, the pressure, $\mathbf{k}$, an external body force such as the earth gravity vector, $\mathbf{g}$, and $\mathbf{T}$, the capillary stress tensor and, T, the temperature field. The density and viscosity as well as the specific heat capacity at constant pressure, c_p, and the thermal conductivity, k, are assumed to be constant for each of the two fluids but may vary across the sharp interface region separating the two phases, depending upon the topology of the flow field. At the interface between the two phases it is necessary to consider the capillary stress tensor $\mathbf{T}$ in order to describe the interaction between the two fluids. Therefore $\nabla \cdot \mathbf{T}$ is computed by the conservative continuous surface stress (CSS) method, given by Lafaurie et al. [7]. The periodical valve acceleration vector, $\mathbf{a}_v(t)$, is added as an external, time dependent body force vector, to the persistent earth gravity vector, such that $\rho\mathbf{k} = \rho(\mathbf{a}_v(t) + \mathbf{g})$. Buoyancy effects driven by temperature gradients were neglected due to the high valve acceleration amplitude and the high frequency of the periodical valve movement.

To identify the topology of the two-phase flow and the advection of the liquid surface, it is necessary to consider its temporal and spatial evolution. The volume-of-fluid (VOF) method described by Harlow and Welch [3] is adequate for this. An additional advection equation for the volume of (liquid phase) fluid fraction f:

$$\frac{\partial f}{\partial t} + \nabla \cdot (\mathbf{u} f) = 0, \tag{4}$$

describes the temporal and spatial evolution of the two-phase flow within the computational domain. The presence of liquid or gas is found by evaluating the value of the VOF-variable defined by:

$$f(\mathbf{x}, t) = \begin{cases} 0 & \text{outside the liquid phase} \\ 0 < f < 1 & \text{at the interface} \\ 1 & \text{inside the liquid phase} \end{cases} \tag{5}$$

Properties of the flow are updated at each time as follows:

$$\rho(t, \mathbf{x}) = \rho_g + (\rho_l - \rho_g) f(t, \mathbf{x}), \tag{6}$$

$$\mu(t, \mathbf{x}) = \mu_g + (\mu_l - \mu_g) f(t, \mathbf{x}), \tag{7}$$

where the subscript g denotes the gas phase and l the liquid phase. The governing equations are solved numerically using a spatial discretization based on a finite volume scheme on a staggered Cartesian grid. The non-linear convective transport is based on a Godunov type scheme in combination with an operator splitting method introduced by Strang [16]. This discretization is second-order accurate, due to the second-order upwind approximation for the convection terms and central differences elsewhere. The formulation for the fully conservative momentum convection and the volume fraction transport, the momentum diffusion, as well as the surface tension is treated explicitly. Also time integration is realized by an explicit Euler (first order) integration scheme at reasonable small time steps. These numerical schemes are described in full detail by Rieber [11].

The numerical scheme to solve the Navier–Stokes equations is based on a two-step projection method proposed by Bell et al. [1]. First, the momentum equation without the pressure gradient is solved explicitly for an intermediate velocity field. That includes the convective and diffusive terms. In order to satisfy the incompressibility constraint that results in a divergence free velocity field, $\nabla \cdot \mathbf{u} = 0$, the pressure field is calculated implicitly from the Poisson equation during the second "projection" step, which completes the scheme. To suppress numerical smearing of the liquid phase for each time step, the interface is reconstructed by the piecewise linear interface calculation method (PLIC) from Rider and Kothe [10]. Then, the volume flux of the liquid phase is convected on the basis of its reconstructed distribution.

Due to the implemented projection method a robust multigrid solver based on a Galerkin coarse grid approximation is used to invert the Poisson equation for the pressure. The discontinuous coefficients resulting from the discontinuous density field and the high density ratio between the two fluids usually cause numerical difficulties and require therefore an efficient smoothing algorithm. To meet these requirements the Red–Black Gauss–Seidel smoother with several pre-and post-smoothing steps in combination with the W-cycle scheme is used and Gauss elimination is applied to solve the equation system on the coarsest multigrid level. In order to increase the stability and reduce the computational effort of the iterative Red–Black scheme, it is automatically optimized by adjusting the number of pre-and post-smoothing steps during runtime, depending on the convergence rate of the multigrid scheme.

Once the velocity vector, $\mathbf{u}$, and the fluid topology, f, is updated the temperature field, T, can be calculated separately since the energy equation (Eq. (3)) is decoupled from Eqs. (1) and (2) due to the incompressibility assumed and the constant fluid properties of each single phase. To compute the temperature field, the convective and the heat conducting terms are considered separately. The procedure solves in a first step the convective term, to obtain an intermediate result of the temperature field, which is based on the volume flux calculated during the advection step of f. In a second step the final temperature field is calculated based on the diffusive heat flux and the present topology of the flow field.

The presented methods were implemented in the 3D-CFD inhouse program Free Surface 3D (FS3D) which has been used to simulate the heat and mass transfer in the present study. Detailed information about the implemented numerical schemes are given by Rieber [11] and Hase [4]. The performance of the program is shown by Rieber and Frohn [12,13] and Sander and Weigand [14]. It allows extensive computational setups due to its interprocess communication capability based on the Message Passing Interface (MPI) and high vectorization ratios on high-performance computing platforms.

3. Numerical setup

3.1. Computational domain and discretization

The geometry of the hollow valve stem, shown in Fig. 2, was defined as a rectangular channel with a square cross section. The extent of the domain varied depending upon the aspect ratio of the valve geometry between $L/H = 14$, 24 and 33 which resulted in a volume of $V = LH^2$ and the corresponding fill level based on the volume V, ranging between 30% and 60%. Different aspect ratios were defined by adapting (i) the valve's length to $L' = 14/24L$ in the cases where $L/H = 14$ and (ii) the valve's height to $H' = 24/33H$ for cases where $L/H = 33$. The computational region was spatially resolved using a uniform rectangular grid with minimum spacing of $H/24$ which resulted in $336 \times 24 \times 24$, $576 \times 24 \times 24$, or $792 \times 24 \times 24$ grid points, respectively. To study the influence of the spatial discretization a refined mesh was used for the cases $L/H = 14$ and 24 with $448 \times 32 \times 32$ and $1152 \times 48 \times 48$ grid points, respectively. For 2D simulations the spatial resolution was refined from 768×32 to 1536×64 and 3072×128 grid points.

On all four side walls and on the end walls, Dirichlet boundary conditions were defined for the velocity corresponding to a no-slip rigid wall condition. To specify the thermal operating conditions, the bottom wall face was defined to operate at a high temperature T_h that appears in the combustion chamber, whereas the upper wall face reached a low temperature T_0 in the region of the camshaft. Neumann boundary conditions, representing adiabatic wall

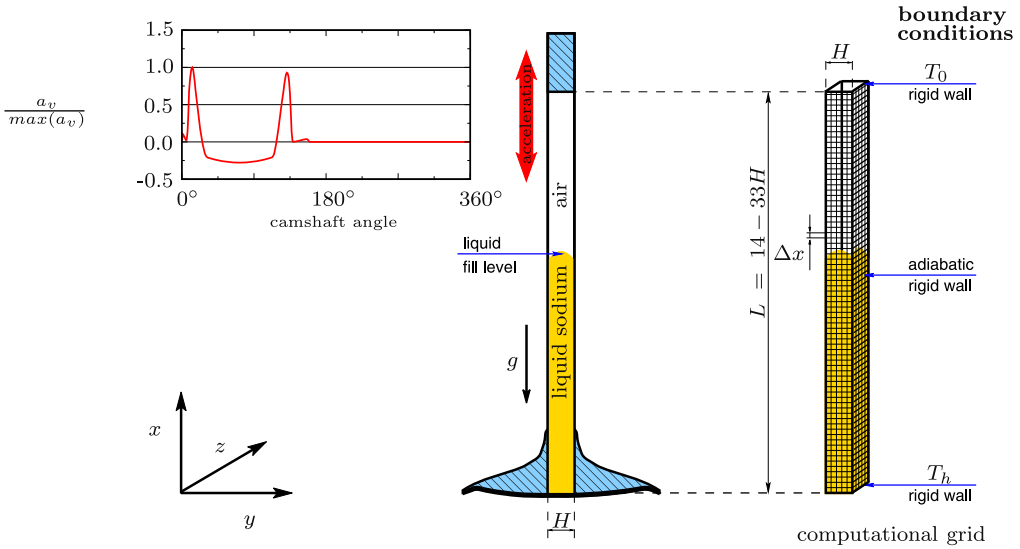

Fig. 2. Vertically installed valve – computational domain and grid.

conditions, which are a simplification compared to the real non-adiabatic walls, were applied on the side walls. To complete the numerical setup, the liquid fill level is initialized according to a vertical installation of the valve, almost identical to the setup shown in Fig. 2 (right).

3.2. Fluid properties

All relevant fluid properties used for the present study are given in Table 1. For the data of air and liquid sodium taken from Fink and Leibowitz [2] an average temperature of 700 K in the system has been assumed. Regarding these properties in detail it is necessary to note the high surface tension and the thermal conductivity which corresponds to a low Prandtl number of 4.96×10^{-3} typical for liquid metals such as liquid sodium. It can be expected that these properties greatly influence the heat transfer in the system. Therefore, it can be concluded that the majority of the total amount of heat flux is caused by conduction and only a minor amount by turbulent fluctuations (see also [5]). In addition, the very high density ratio $\frac{\rho_l}{\rho_g} \approx 1700$ between the two fluids must be considered since it generally causes numerical difficulties for standard numerical solvers (see [8]).

3.3. Valve acceleration

The typical movement and acceleration of an engine valve is shown in Fig. 3. Due to the high rotational speed of modern combustion engines (≈6000 rpm), a very high valve acceleration with an order of magnitude of approximately 1000g is generated depending on the valve lift. Based on the characteristic shaking movement of the valve, a strong mixing effect in the valve must be expected during the opening and closure period. This is followed by an acceleration free, stationary period during the compression and combustion process in the cylinder. To include the typical movement of the valve lift and the corresponding velocity, the time dependent acceleration function following the shape shown in Fig. 3 is derived and introduced as an external body force (see Eq. (2), $\rho\mathbf{k} = \rho(\mathbf{a}_v(t) + \mathbf{g})$).

Table 1
Fluid properties at 700 K.

Fluid properties	Liquid sodium	Air	Units
Density ρ	852	0.503	kg/m^3
Viscosity μ	2.64×10^{-4}	3.332×10^{-5}	kg/m s
Surface tension σ	166.2	–	mN/m
Specific heat capacity c_p	1277	1075.2	J/kg K
Thermal conduction k	68	0.0523	W/m K
Prandtl number Pr	4.96×10^{-3}	0.685	–

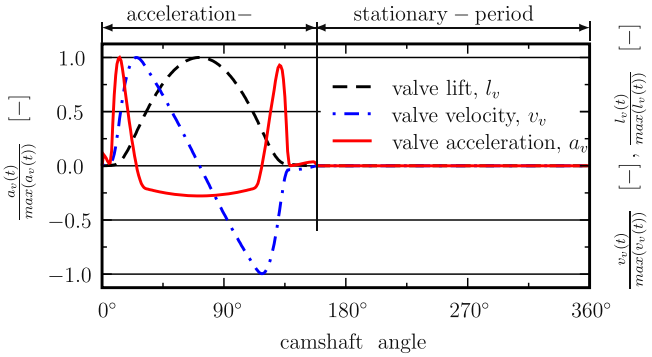

Fig. 3. Valve movement.

4. Influence of the numerical discretization

In the present study mostly three-dimensional effects were considered in order to identify the differences caused by a simplified two-dimensional setup which has been regarded earlier (see [15]). Due to the enhanced computational resources several three-dimensional simulations were performed in order to demonstrate the highly three-dimensional character of the flow. In addition to these simulations the influence of the spatial resolution was considered which is discussed in the following.

4.1. Influence of the spatial discretization

Since the present numerical approach excludes any turbulence modeling based on the idea to capture all fluctuations in the flow by an extremely fine spatial resolution, the grid spacing must be adequate. To meet this requirement the resolution must be at least in the order of the dissipative length scale which is the Kolmogorov length scale (see [9]). Compared to widely studied fully developed

pipe flows or similar flows, the nature of the flow type in the present study appears to be much more complicated. The highly transient character of this two phase flow is one of the main reasons for the difficulties to determine the order of the dissipative length scale. Regarding the Reynolds number (Fig. 4) $Re_H = (\rho v^{rms} H)/\mu_l$ which is based on the rms-velocity, v^{rms}, of the flow field, and the hydraulic diameter ($D_h = H$) in the square channel, the highly transient character of the flow can be seen. Additionally, the size of the ligaments shown in Fig. 7 requires also a fine spatial resolution in order to capture the nature of the two-phase flow correctly.

To overcome this question, the case of $L/H = 14$ was simulated by using a refined mesh with a spacing of $H/32$. In Fig. 4 the different outcome considering the temporal evolution of the kinetic energy and the mean temperature of the liquid phase as well as the heat flux in x-direction is shown. In particular the heat flux differs which can be explained by the different size of the ligaments due to the refined mesh. The different results depending on the grid resolution are also shown in Fig. 5. Although the qualitative outcome during the stationary period is very similar, the dependency of the ligament size on the spatial resolution can be identified in particular during the acceleration period. This explains the differences appearing for the heat flux in x-direction since the heat transfer depends on the coalescence and merging of hot and cold ligaments as well as the size of the ligaments (see also details c, c' and d, d' or e in Fig. 8).

4.2. Influence of 2D vs. 3D discretization

In addition to the influences caused by the spatial discretization significant differences were also observed between the results of two- and three-dimensional setups. Although the character of the flow is very similar, the clustering of the liquid was not observed in a two-dimensional setup. The level of the averaged quantities shown in Fig. 6 differs also due to the simplified two-dimensional setup. The comparison at a fill level of 40% shows that the kinetic energy is underpredicted in a two-dimensional setup and the heat flux is overpredicted compared to the three-dimensional setup. Particularly at a fill level of 60% a very high heat flux appears compared to the other cases with lower liquid fill levels which is not the case in a three-dimensional setup (see Fig. 11). This indicates that a simplified two-dimensional setup generally overpredicts the heat flux compared to the three-dimensional setup. This phenomenon can be caused by the clustering which is mostly absent in a two-dimensional setup and therefore influencing the liquid bridging between the hot and cold valve ends. Thus, it can be concluded that the two-dimensional approach is only able to predict the qualitative character of the flow. However, since three-dimensional effects have a dominating influence, it is necessary to use three-dimensional setups. The computational requirements in the present case are roughly 10 times higher compared to a two-dimensional setup, which reflects the advantage of a simplified two-dimensional setup.

5. Results

This study focuses on identifying and analyzing the appearance of flow phenomena caused by different influencing factors. Therefore all simulations used identical thermal boundary conditions and constant liquid properties (see Table 1). The results previously discussed which were obtained by using different grid resolutions have shown the influence of the spatial discretization within the present study. For the following results, we varied and studied independently the influence of the liquid fill level, the geometrical dimensions of the valve and the acceleration acting on the system. This section illustrates the appearing three-dimensional flow phenomena and the inherent heat transfer mechanisms during the engine operation cycle. It is followed by regarding the influence of the considered factors which is discussed by evaluating the temporal evolution of the kinetic energy, the heat flux and the average temperature in the system.

5.1. Three-dimensional characteristics of the flow and temperature field

Since the topology of the flow field is strongly dominated by the valve's movement, the following section is dedicated to identify the characteristic flow phenomena appearing inside the valve during engine operation. The temporal evolution of the complex three-dimensional topology of the two-phase flow is shown for a valve at a fill level of 50% and $L/H = 33$. The corresponding velocity field as well as the temperature field and the heat flux is considered for this specific case since it is characteristic for the flow phenomena of all cases. Therefore, several three-dimensional views and details

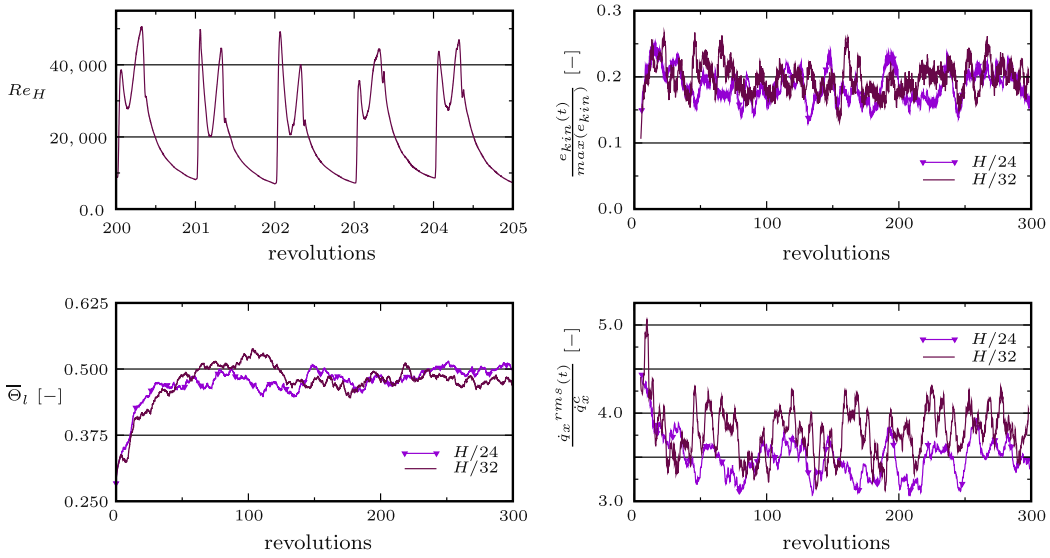

Fig. 4. Case $L/H = 14$ at a resolution of $H/32$ vs. $H/24$. Temporal evolution of the Reynolds number (top-left) and temporal evolution of the averaged liquid phase kinetic energy (top-right). Averaged rms-value of the heat flux in axial (x) direction (bottom-right) and liquid temperature (bottom-left).

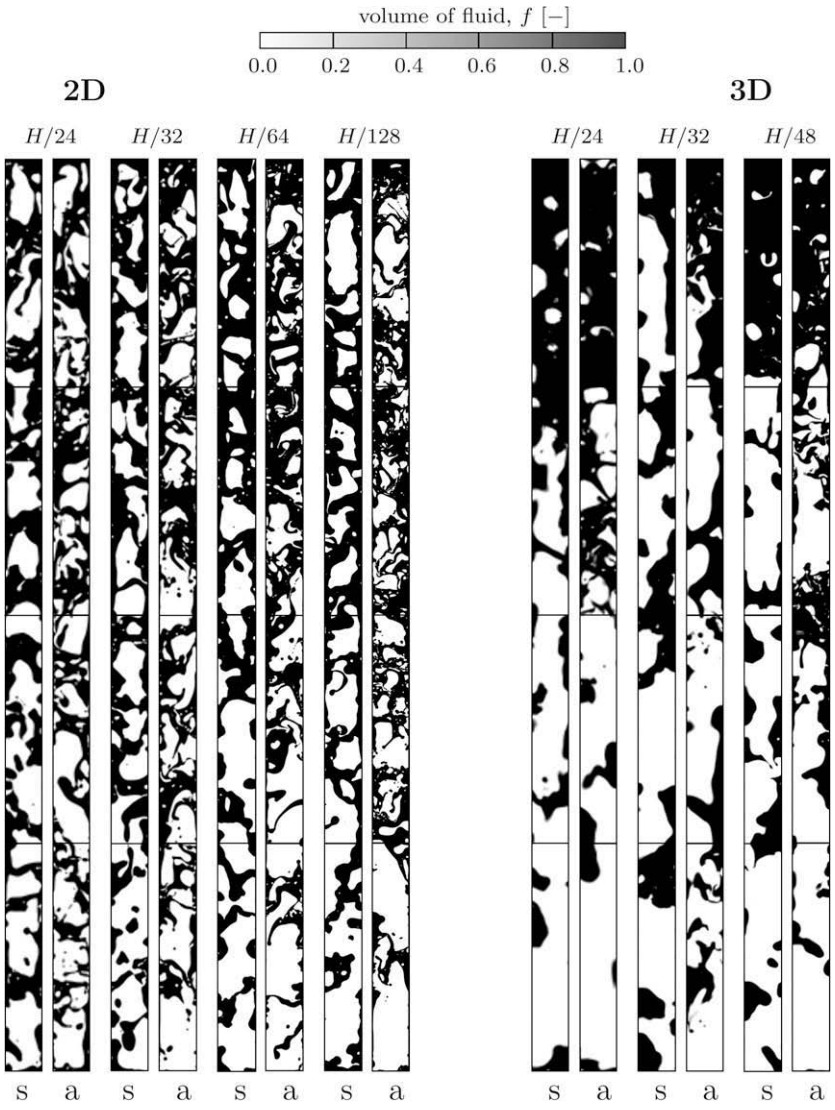

Fig. 5. Instantaneous view of the fluid topology during the acceleration (a) at 0° and stationary (s) period at 90° according to different spatial resolutions – 2D vs. 3D simulation results, domain size: $24H \times H$.

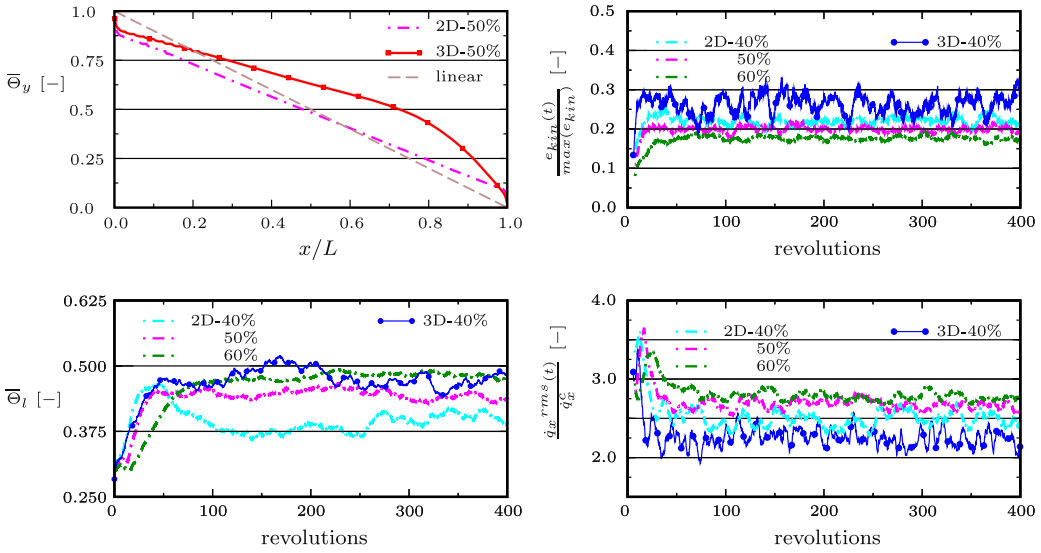

Fig. 6. 2D vs. 3D simulation results in the case $H/D = 24$. Temporal evolution of the averaged liquid phase kinetic energy (top-right). Averaged rms-value of the heat flux in x-direction (bottom-right) and mean liquid temperature (bottom-left).

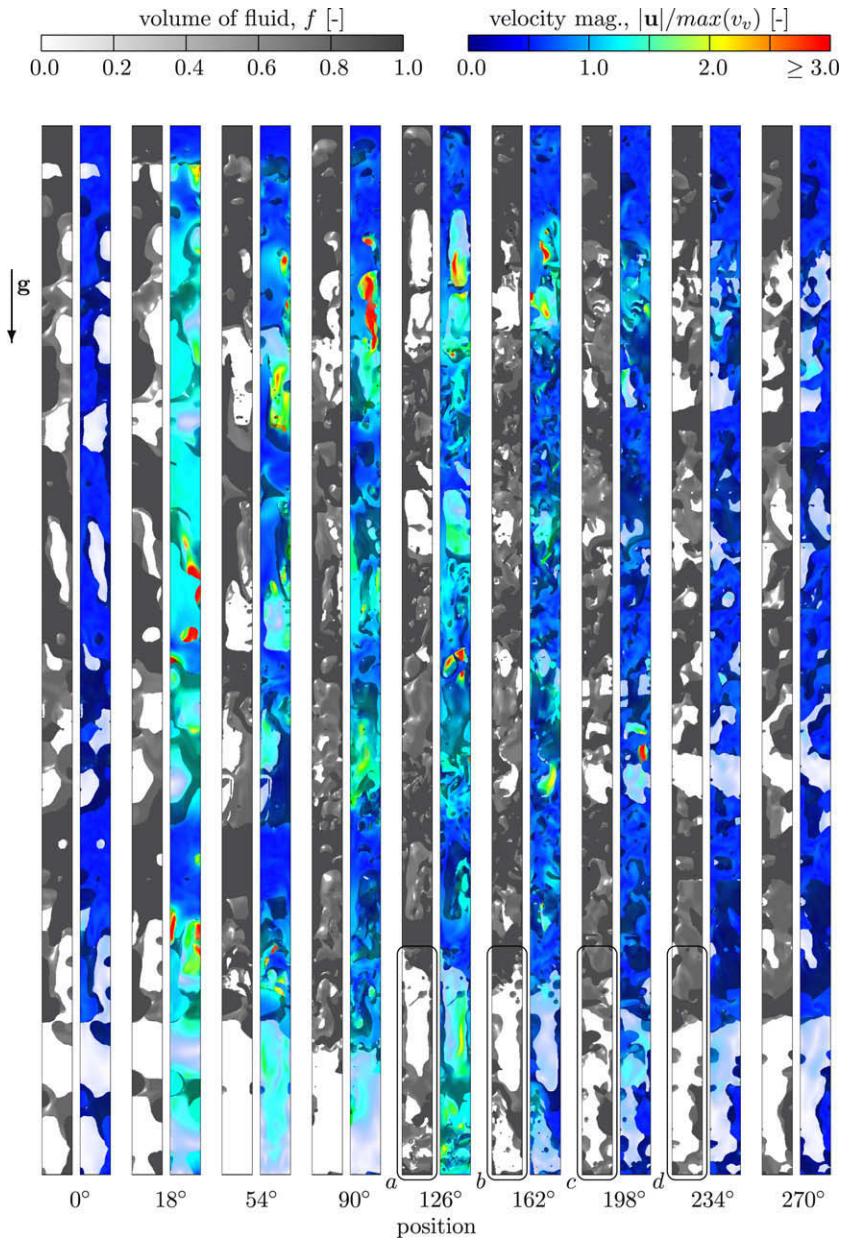

Fig. 7. Instantaneous 3D-view (from $H/2$ to H in z-direction) of the fluid topology and the velocity magnitude during one revolution – 3D domain size: $33H \times H \times H$, grid size: $792 \times 24 \times 24$. GPU-based Ray Casting (see [6]).

of the flow field are shown and discussed at certain points in time during one revolution. The temporal development of the three-dimensional flow during the acceleration and stationary period from cycle 200 to 201 is shown in Fig. 7.

The complex topology changes in the liquid phase and the velocity magnitude of the flow field can be identified. This indicates that the nature of the transport mechanisms appearing must be highly transient and three-dimensional. In Fig. 7 the strong coupling of the fluid fragmentation and the velocity field of the two-phase flow during the valve movement can be observed. In particular the acceleration period at positions 18°, 54°, 90°, 126° and 162° results in high local velocity magnitudes and small liquid ligaments (see details *a* and *b*). During the following stationary period at 198°, 234° and 270° or later, the ligament size grows again due to the collisions appearing between the numerous small ligaments present inside the valve (see details *c* and *d*). At the same time the velocity magnitude is reduced since the flow is only driven by inertial forces.

The corresponding heat transfer mechanisms based on convective mixing effects and thermal diffusivity are clearly visible in Fig. 8. At certain positions during one revolution it can be recognized that liquid at the bottom heats up and convects the heat towards the center of the valve (see details *a* and *b* at positions 0° and 18°). Simultaneously, the liquid at the top is cooled down by contacting the upper wall and convects towards the center of the valve. The temperature between the hot and cold ligaments is balanced by means of heat conduction and liquid mixing since liquid ligaments undergo collisions and fragmentations during the engine operation cycle. This transport mechanism and the mixing of hot and cold liquid bridges the two valve ends and changes the temperature profile in axial direction very efficiently compared to a system which is based solely on conduction.

The high heat flux quantities appearing inside the liquid flow indicate the efficiency of the liquid sodium heat-carrying. Especially at the cold side of the valve stem, where many ligaments are cumulated, and across the center of the valve stem, high heat

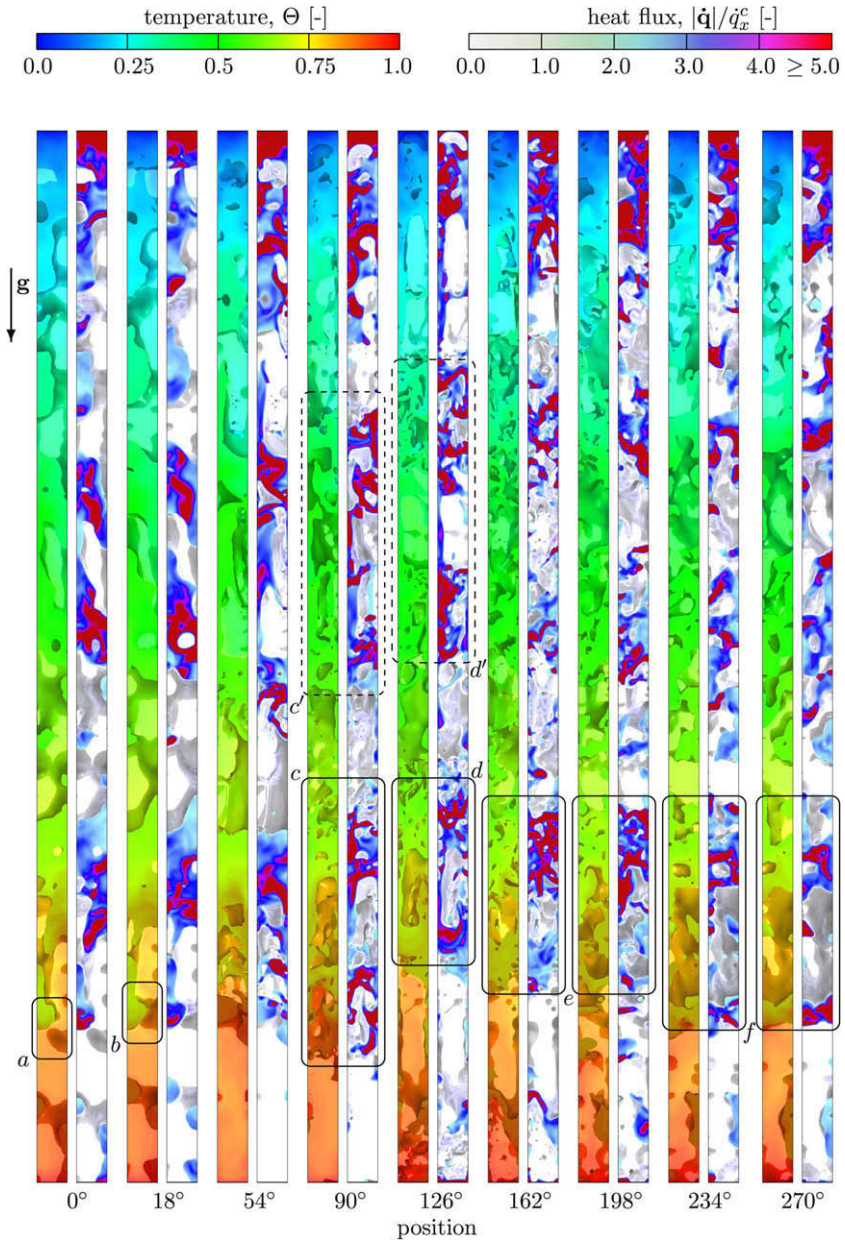

Fig. 8. Instantaneous 3D-view (from $H/2$ to H in z-direction) of the temperature field and the heat flux during one revolution-3D domain size: $33H \times H \times H$, grid size: $792 \times 24 \times 24$. GPU-based Ray Casting (see [6]).

flux rates are achieved. The heat flux at the hot bottom wall of the valve is low due to the low liquid mass in this region and the weak heat transfer inside the air. It can be seen that the size of the ligaments is also responsible for an effective heat transfer which is observed at positions 90°, 126° and 162° (see details *c*, *c′* and *d*, *d′* or *e*). Additionally it can be identified that several ligaments have very low heat flux rates, which indicates a uniform temperature inside the ligament. At the same time ligaments with high heat flux rates caused by collision of hot and cold liquid ligaments and the ongoing temperature balancing (see details *e* and *f* at positions 198°, 234° and 270°) can be identified. In addition to this it was observed that the flow is quite incoherent from cycle-to-cycle, which indicates that flow topology variations during one revolution are very strong.

The presented field values indicate the appearing mechanisms and the influence of the shaking movement of the valve. Thus, the nature of the valve movement, the geometrical dimensions and of course the liquid fill level are influencing parameters which are considered in detail later in this section. First the results for the kinetic energy, temperature and heat flux are presented.

5.2. Averaged integral values

In order to identify the efficiency of the shaker-based transport it is necessary to reduce the three-dimensional data to simple quantities which can be compared individually for each setup. The most significant quantities in this context are the kinetic energy and the heat flux in axial direction as well as the mean temperature inside the whole system. These values were obtained from the computed field values and averaged at each time step for each phase separately.

5.2.1. Kinetic energy

The kinetic energy of the liquid phase clearly represents the convective part of the transport mechanism. Due to different geometrical dimensions and different liquid fill levels, the fluid topol-

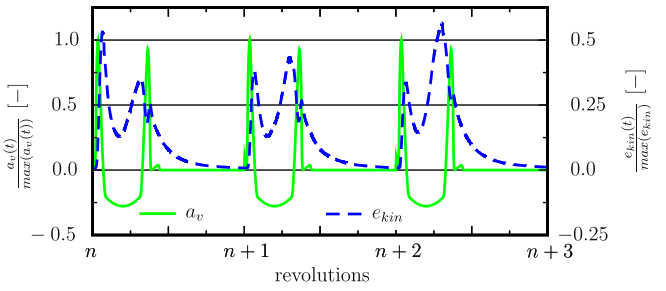

Fig. 9. Temporal evolution of the liquid phase kinetic energy vs. valve acceleration at a liquid fill level of 50% and $L/H = 33$.

ogy can vary drastically. According to Fig. 9 it can be recognized directly that the kinetic energy of the liquid mass, m_l, averaged over the complete volume, follows the nature of the valve acceleration. The kinetic energy is normalized by the maximum level of the kinetic energy, based on the following relation $\max(e_{kin}) = 1/2 m_l \max(v_v^2)$. The typical movement is characterized by the acceleration period where high levels of kinetic energy are reached in the order of $\geqslant 0.125$ and low levels in the order of $\leqslant 0.125$ during the stationary period, where only the inertial motion appears.

It can be concluded that the periodic nature of the acceleration is the driving mechanism for the convective process inside the valve which introduces a high amount of kinetic energy during the acceleration period. This is followed by the stationary period, which is dominated by the deceleration of the flow due to viscosity and coalescence effects (see Fig. 7).

5.2.2. Temperature

The temperature field inside the valve is a result of the heat transfer mechanisms appearing between the hot and the cold valve ends and the adiabatic side walls. By averaging the field data over 400 revolutions the temporal evolution of the fluid topology and the corresponding temperature field is found (see Fig. 10). It can be observed that a major part of the liquid mass, indicating the wetted region, is clustered in the upper cold region of the valve stem. This behavior also leads to an higher temperature gradient in this region which can be identified by regarding the trend obtained from averaging the 2D-temperature field in y-direction.

Compared to the trend expected for a valve at a fill level of 100% (solid slab) where heat transfer is only based on heat conduction a clear difference can be noted. The temperature field is following the trend given by Eq. (8), where $a = (\rho/c_p k)_l$

$$\Theta = \frac{T - T_0}{T_h - T_0} = \mathrm{erfc}\left(\frac{x}{2\sqrt{at}}\right) \tag{8}$$

represents the thermal diffusivity, for a semi-infinite plate. Until $T(x/L = 1.0) = T_0$ the results can be compared directly and for a late stage the linear trend of the temperature field between the two walls appears.

Differences between these two setups appear particularly at the hot valve side, $(x/L = 0.0)$, where the averaged temperature at a fill level of 50% is lower and at positions $(x/L > 0.5)$ where the averaged temperature is higher. The lower temperature level achieved at the hot side demonstrates the cooling efficiency of a shaker-based cooling technique compared to a system which is based on heat conduction only. The higher temperature level at positions $x/L > 0.5$ and the increased temperature gradient normal to the wall allows higher heat transfer rates over the side wall which is not adiabatic in reality.

The temporal evolution of the temperature field reaches a quasi-stationary state where the heat flux introduced at the lower, hot wall is balanced by the heat flux passing at the upper cold wall. The evolution of the averaged heat flux is shown in Figs. 11 and 13 as well as the liquid temperature shown in Figs. 12 and 14. Details regarding the calculation of the heat flux in the system are given in the following.

5.2.3. Heat flux

Since the internal heat transfer is relevant for the cooling process, it is necessary to identify the amount of heat transferred in x-direction. The heat flux, $\dot{q}_{x_{ijk}}$, in this direction is computed every time step as

$$\dot{q}_{x_{ijk}} = -k_{ijk} \frac{\Delta T_{ijk}}{\Delta x_{ijk}} \tag{9}$$

based on the fluid topology and the temperature field in each computational node, (i,j,k), on the equidistant grid used. To reduce the field data, root mean square values are calculated every timestep according to the following relation:

$$\dot{q}_x^{\mathrm{rms}}(t) = \sqrt{\frac{1}{N} \sum_{ijk} \dot{q}_{x_{ijk}}^2}. \tag{10}$$

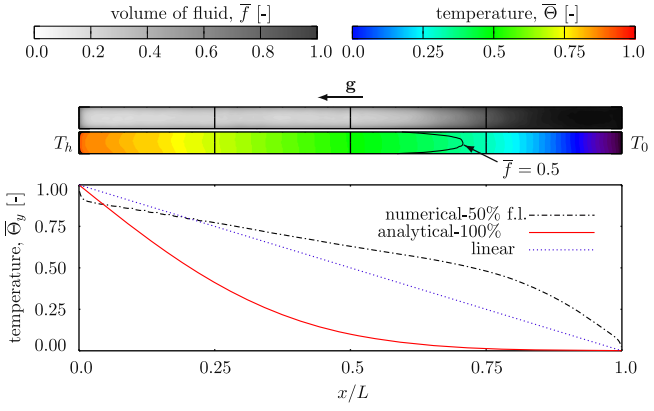

Fig. 10. 2D-view at $z = H/2$ of the fluid topology and the temperature field at a fill level of 50%, averaged over 400 revolutions compared to the analytical solution for a fill level of 100% – 3D domain size: $24H \times H \times H$, grid size: $576 \times 24 \times 24$.

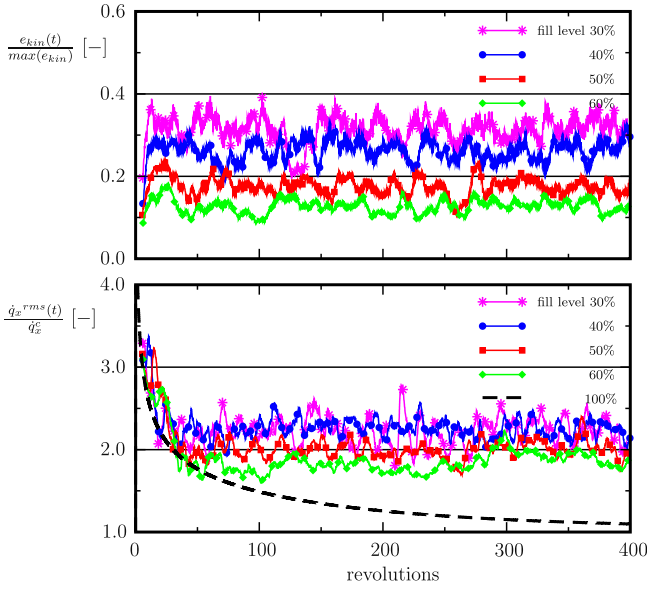

Fig. 11. Temporal evolution of the averaged liquid phase kinetic energy (top) and the averaged rms-value of the heat flux in axial (x) direction (bottom) at different fill levels in a $L/H = 24$ valve.

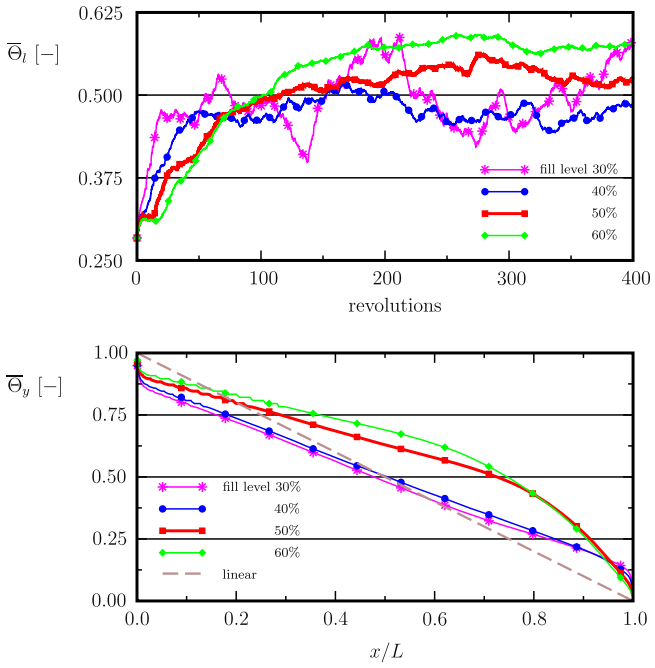

Fig. 12. Temporal evolution of the mean liquid temperature (top) and spatial distribution of the averaged temperature after 400 revolutions in y-direction (bottom) at different fill levels in a $L/H = 24$ valve.

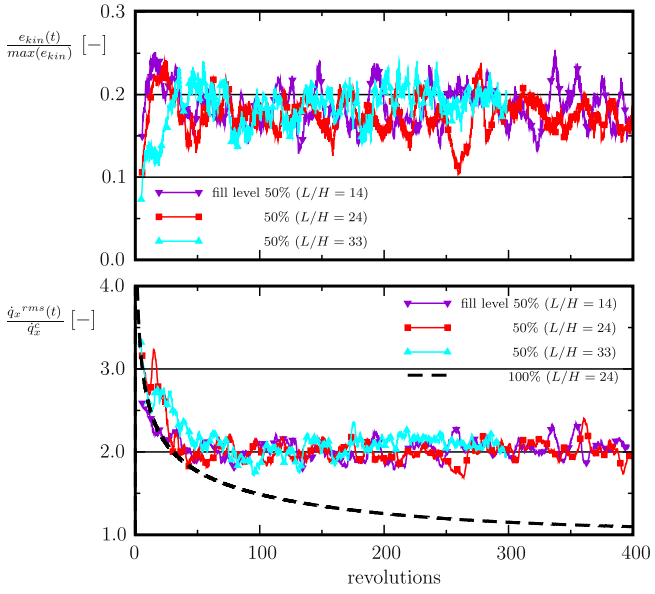

Fig. 13. Temporal evolution of the averaged liquid phase kinetic energy (top) and the averaged rms-value of the heat flux in axial (x) direction (bottom) at different geometrical dimensions.

The rms-value of the x-heat flux $\dot{q}_x^{rms}$ shown in Figs. 11 and 13 as well as Figs. 16, 4, and 6 is averaged and normalized by the heat flux based on conduction, $\dot{q}_x^c = -k(T_h - T_0)/L$, which corresponds a valve at 100% fill level. Since the heat flux depends on the mixing mechanisms of hot and cold ligaments, a strong influence of the flow characteristics must be expected, which is discussed in the following.

5.3. Influence of the liquid fill level

The liquid fill level is a major influencing parameter with respect to the transport phenomena appearing during the valve movement. Once the fill level is too high the convective transport mechanisms break down due to the high liquid mass and the corresponding collision frequency of the ligaments. A reduced liquid level increases the convective transport but at a certain limit it breaks down too, due to the limitations considering its carrier function. This results in a weak liquid bridging between the hot and cold valve ends.

An optimal fill level would therefore lead to highest levels of kinetic energy and heat flux simultaneously. According to Fig. 11 the normalized levels of kinetic energy range between values of 0.1 at 60% fill level up to 0.4 at a fill level of 30%. The normalized rms-value of the heat flux shown in Fig. 11 reaches values approximately twice as high compared to the heat flux based on conduction only (100% fill level). The different levels of kinetic energy and heat flux clearly indicate that the liquid fill level influences the heat transfer inside the valve. At a fill level of 30–40% highest values of kinetic energy and heat flux are achieved. The values reached at a fill level of 50–60% are lower.

The temporal evolution of the mean liquid temperature $\overline{\Theta}_l$, shown in Fig. 12, reaches levels of $\overline{\Theta}_l > 0.5$ at fill levels of 50–60%. At fill levels of 30–40% the trend of the mean liquid temperature is lower ($\overline{\Theta}_l < 0.5$). In addition high fluctuations of the mean liquid temperature can be observed at 30% fill level which indicates that the liquid bridging is weaker at a low fill level. The averaged temperature field after 400 revolutions in vertical direction, $\overline{\Theta}_y$, varies also, depending on the fill level. Compared to the linear trend of the temperature distribution in axial direction, fill levels between 50% and 60% lead to an overall higher temperature, except the hot valve end. The lower temperature levels observed in this region demonstrate the efficiency of the shaker-based cooling mechanism. At a fill level of 30–40% the averaged temperature is below the linear trend in the region $0 \leqslant x/L \leqslant 0.5$ and higher where $0.5 \leqslant x/L \leqslant 1.0$. This indicates again, that lower liquid fill levels of 30–40% lead to a better thermal efficiency of the complete system.

5.4. Influence of the valve geometry

To identify the influence related to the geometrical dimensions of the valve stem, the flow inside the valve at aspect ratios ranging

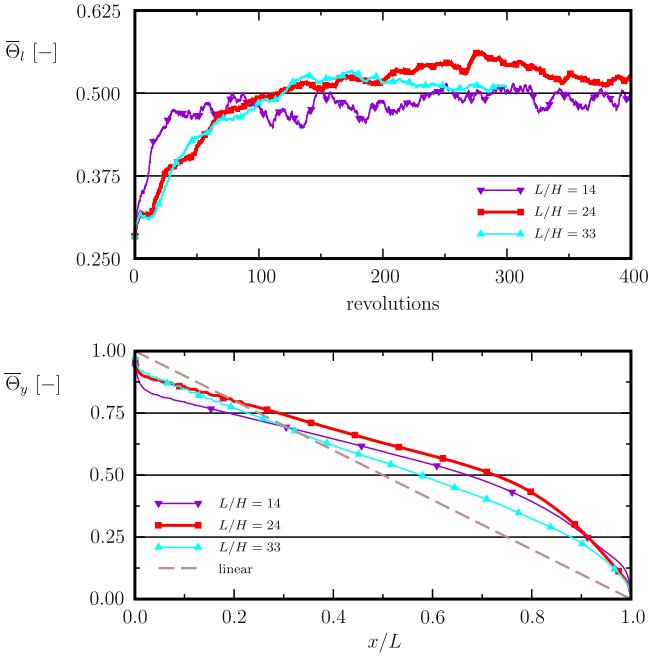

Fig. 14. Temporal evolution of the mean liquid temperature (top) and spatial distribution of the averaged temperature after 400 revolutions in y-direction (bottom) at different geometrical dimensions and a liquid fill level of 50%.

from $L/H = 14$, 24 or 33 and a constant liquid fill level of 50% was considered. The temporal evolution of the relevant quantities such as the kinetic energy and the heat flux shown in Fig. 13 indicate that only minor differences appear. This result shows that obviously no serious influence on the efficiency of shaker-based cooling must be expected if the geometrical dimensions are changed within the presented range or beyond.

However, the temporal evolution of the liquid temperature in Fig. 14 shows some relevant differences. It can be seen that the heating of the liquid is much faster at $L/H = 14$ compared to $L/H = 24$ or $L/H = 33$. This fact indicates that the convective transport during the first 100 revolutions is faster compared to other configurations which are also visible by regarding the trend of the kinetic energy. The trend of the averaged liquid temperature tends for all configurations towards $\overline{\Theta}_l = 0.5$ whereas the configurations $L/H = 24$ at a fill level of 60% and 50% are above 0.5. Due to the strong transient character of the flow it is not possible to exactly determine constant values for $\overline{\Theta}_l$. Since the temperature inside the valve indicates the cooling efficiency of the system it can be identified that a liquid fill level of 40% ($L/H = 24$) and a lower aspect ratio ($L/H = 14$) at a fill level of 50% enhance the cooling efficiency.

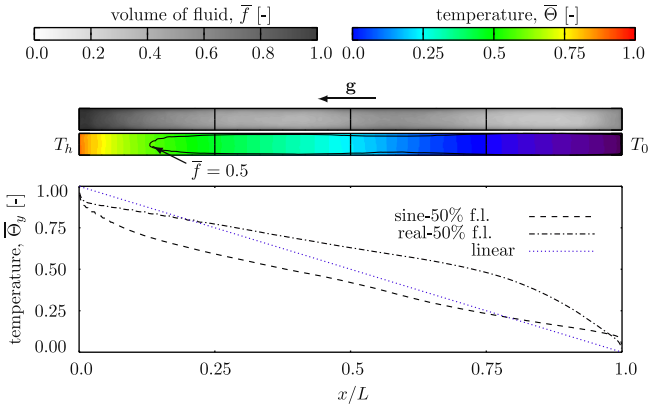

Fig. 15. 2D-view at $z = H/2$ of the fluid topology and the temperature field at a fill level of 50%, averaged over 400 revolutions compared to the analytical solution for a fill level of 100% – 3D simulation results with sinusoidal acceleration, domain size: $24H \times H \times H$, grid size: $576 \times 24 \times 24$.

The spatial distribution of the temperature field averaged over 400 revolutions results in similar trends although some minor differences are visible in Fig. 14 (bottom). Finally, it can be concluded that the aspect ratio of the valve stem is not a dominating influencing factor such as the liquid fill level, which allows to optimize the geometrical dimensions of the valve on other specifications and requirements.

5.5. Influence of the valve acceleration

Since the focus of the present study was directed to identify different influencing parameters, the valve acceleration must be considered as well. The clustering of the liquid mass shown in Fig. 10 was one of the reasons to study a sinusoidal acceleration type (see Fig. 16) because it was assumed that the character of the acceleration is causing this phenomenon. The resulting flow and temperature field, averaged over 400 revolutions, is presented in Fig. 15. Regarding the averaged distribution of $\bar{f}$, it can be identified that clustering at the cold valve end is not longer present. In fact, a weak clustering appears at the lower, hot valve end. This indicates that the character of the acceleration is obviously influencing the clustering tendency. The corresponding spatial distribution of the averaged temperature field shows a more linear trend at a lower temperature level compared to the outcome of a realistic valve acceleration.

The trends of the temporal evolution of the averaged quantities (Fig. 16) such as the kinetic energy or the heat flux in axial direction are slightly higher for the sinusoidal acceleration type compared to the real acceleration. However, the differences are small which indicates that the amount of kinetic energy introduced by the changed sinusoidal acceleration is similar to the real acceleration. The final outcome of the averaged mean liquid temperature $\overline{\Theta}_l$ tends again towards a value of 0.5.

5.6. Clustering and temporal breakdown

One significant phenomenon appearing besides the clustering of the liquid is the development of the averaged temperature field which suddenly can increase or decrease within a few revolutions. This behavior can be interpreted as a temporal breakdown of the shaker-based cooling mechanism if $\overline{\Theta}$ increases which is more critical than cases where $\overline{\Theta}$ decreases (see Fig. 17). Since a temporal

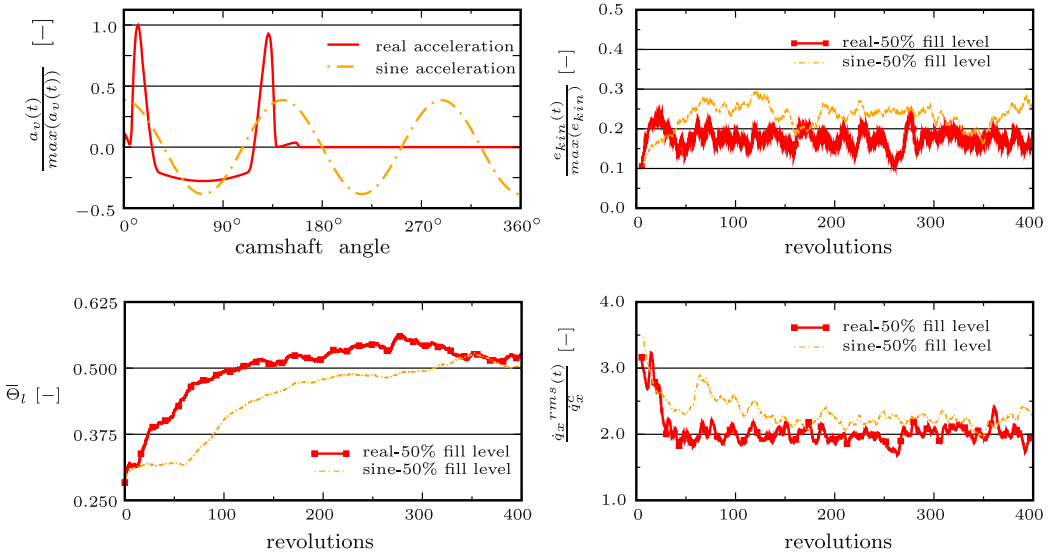

Fig. 16. Valve acceleration – sinusoidal vs. realistic acceleration (top-left). Temporal evolution of the averaged liquid phase kinetic energy (top-right), the averaged rms-value of the heat flux in axial (x) direction (bottom-right) and mean liquid temperature (bottom-left).

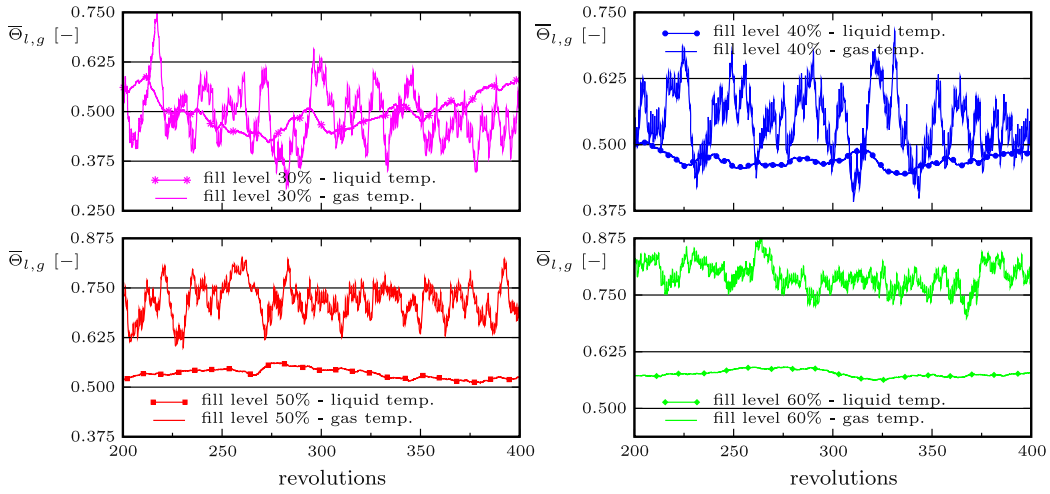

Fig. 17. Temporal evolution of the mean liquid and gas temperature at different fill levels and $L/H = 24$.

breakdown of the regarded mechanisms results in high thermal loads and eventually leads to a burn-out of the valve it appears important to reflect the flow appearing in greater detail. The resulting temporal evolution of the mean temperature, according to different fill levels in the case where $L/H = 24$, is shown in Fig. 17. It can be seen that $\overline{\Theta}_{\mathrm{l}}$ and $\overline{\Theta}_{\mathrm{g}}$, the mean liquid and gas temperature, strongly depend on the liquid fill level. This is indicated by (i) the growing temperature difference if the liquid fill level is increased, (ii) the growing fluctuation tendency of the mean temperature with lower liquid fill levels and (iii) the overall growing temperature range at higher fill levels.

In general it can be observed that $\overline{\Theta}_{\mathrm{l}}$ increases if $\overline{\Theta}_{\mathrm{g}}$ is decreasing and vice versa. Furthermore it can be seen that the mean liquid temperature is always lower than the mean gas temperature, in particular at higher liquid fill levels. It can be concluded that the thermal balancing is influenced by the liquid wetting and cooling of the hot valve end. According to this observation, a low liquid fill level appears to cause the strong fluctuations of the mean gas temperature which causes temperature differences in the range of $\Delta\overline{\Theta}_{\mathrm{g}} = 0.375—0.625$ within a few revolutions for a fill level of 30%. Hence, too low liquid fill levels lead to a temporal breakdown if the hot valve region is not wetted regularly by the liquid coolant. Too high fill levels are a restricting factor as well since the mixing mechanism tends to break down due to the frequent collisions appearing. The optimum fill level appears to be in the order of 30–50%.

6. Conclusion

The results of the present study provide a detailed insight into the shaker-based cooling technique of engine valves. It can be identified that the nature of the two-phase flow appearing is dominated by the periodic shaking movement which is caused by the valve acceleration. During the first acceleration period, a strong fragmentation of the coherent liquid structures can be observed. The following stationary period is mainly dominated by inertial forces acting on the flow. Based on the topology changes of the flow field, the inherent temperature field is mainly influenced by the convective but also by the conductive heat transfer since the thermal conductivity of the liquid sodium is very high.

Thus, the efficiency of the cooling system can be determined indirectly, by regarding the convective and conductive amount of heat transferred. This is represented by the kinetic energy in the system and the heat flux in the axial direction. To demonstrate the influence of different parameters several geometrical configurations were studied as well as the influence of the liquid fill level and the nature of the acceleration. It has been shown that the liquid fill level is a dominating influencing factor which is relevant for the cooling efficiency in the system. The clustering phenomena were mainly caused by the typical acceleration type, but it was not observed for a sinusoidal acceleration type. The geometrical modifications in the range of $L/H = 14–33$ resulted in small differences indicating the minor influence of the aspect ratio in this context.

Additional differences caused by the numerical discretization were also considered in order to estimate its influence on the outcome of the present study. In particular 2D-simulations were found to underpredict the level of kinetic energy and overpredict the heat flux compared to 3D-simulations. In addition the clustering phenomena were not observed to the extent found by the three-dimensional discretization. This finally leads to a different outcome of the temperature field. Due to the complex geometry of internally cooled valves, which was not discretized in full detail, the present results should solely be considered in a qualitative manner. In general it would be convenient to use higher spatial resolutions since the flow topology during the acceleration period appears to depend on the spatial resolution. However, the computational requirement for 400 revolutions was in the order of 1500–3000 CPUh on the NEC SX-8 platform, when using a three-dimensional setup.

Acknowledgments

The authors are very grateful for the financial support of MAHLE VALVE TRAIN SYSTEMS for parts of this work and the High Performance Computing Center Stuttgart (HLRS) for support and supply of computational time on the national super computer NEC SX-8 under the Grant No. FS3D/11142. The authors greatly appreciate the efforts by T. Klein from the Institut für Visualisierung und Interaktive Systeme (VIS) at Universität Stuttgart for assisting in the production of Figs. 7 and 8.

References

[1] J.B. Bell, P. Colella, H.M. Glaz, A second-order projection method for the incompressible Navier–Stokes equations, J. Comput. Phys. 85 (1989) 257–283.
[2] J.K. Fink, L. Leibowitz, Thermodynamic and transport properties of sodium liquid and vapor, Technical Report, Argonne National Laboratory, 9700 South Cass Avenue, Argonne, IL 60439, USA, 1995.
[3] F.H. Harlow, J.E. Welch, Numerical calculation of time-dependent viscous incompressible flow of fluid with free surface, Phys. Fluids 8 (12) (1965) 2182–2189.

[4] M. Hase, Numerische Berechnung dreidimensionaler Transportvorgänge an angeströmten sich verformenden Tropfen, Ph.D. Thesis, Universität Stuttgart, 2005.
[5] W.M. Kays, M.E. Crawford, B. Weigand, Convective Heat and Mass Transfer, fourth ed., McGraw-Hill, New York, 2004.
[6] T. Klein, M. Strengert, S. Stegmaier, T. Ertl, Exploiting frame-to-frame coherence for accelerating high-quality volume raycasting on graphics hardware, in: Proceedings of IEEE Visualization'05, IEEE, 2005, pp. 223–230.
[7] B. Lafaurie, C. Nardone, R. Scardovelli, S. Zaleski, G. Zanetti, Modelling merging and fragmentation in multiphase flows with SURFER, J. Comput. Phys. 113 (1994) 134–147.
[8] J. Li, Y. Renardy, M. Renardy, A numerical study of periodic disturbances of two-layer couette flow, Phys. Fluids 8 (12) (1998) 3056–3071.
[9] P. Moin, K. Mahesh, Direct numerical simulation: a tool in turbulence research, Annu. Rev. Fluid Mech. 30 (1998) 539–578.
[10] W.J. Rider, D.B. Kothe, Reconstructing volume tracking, J. Comput. Phys. 141 (1998) 112–152.
[11] M. Rieber, Numerische Modellierung der Dynamik freier Grenzflächen in Zweiphasenströmungen, Ph.D. Thesis, Universität Stuttgart, 2004.
[12] M. Rieber, A. Frohn, Navier–Stokes simulation of droplet collision dynamics, in: Proceedings of the Seventh International Symposium on Computational Fluid Dynamics, 1997.
[13] M. Rieber, A. Frohn, in: Parallel Computation of Interface Dynamics in Incompressible Two-Phase Flows In High-Performance Computing in Science and Engineering 99: Transactions of the High Performance Computing Center Stuttgart (HLRS), Springer, Berlin, 2000, pp. 241–252.
[14] W. Sander, B. Weigand, Direct numerical simulation on the influence of the nozzle design for water sheets emerged at moderate Reynolds numbers, in: High-Performance Computing in Science and Engineering 2007: Transactions of the High Performance Computing Center Stuttgart (HLRS), Springer, Berlin, 2007.
[15] W. Sander, B. Weigand, C. Beerens, Direct numerical simulation of two phase flows in liquid cooled engine valves, in: Proceedings of HT2005, ASME Summer Heat Transfer Conference, San Francisco, USA, 2005.
[16] G. Strang, On the construction and comparison of difference schemes, SIAM J. Numer. Anal. 5 (3) (1968) 506–517.
[17] Wikipedia. Ventiltrieb – Wikipedia, the free encyclopedia. <http://de.wikipedia.org/wiki/Bild:Ventiltrieb.jpg>, 2007 (accessed 08.12.07).